Physica Medica (2008) 24, 204–211

available at www.sciencedirect.com

ScienceDirect

journal homepage: http://intl.elsevierhealth.com/journals/ejmp

Physica

ORIGINAL PAPER

Variation of dose distribution of stereotactic radiotherapy for small-volume lung tumors under different respiratory conditions

E. Kunieda [a,*], H.M. Deloar [b], N. Kishitani [c], T. Fujisaki [c], T. Kawase [a], S. Seki [a], Y. Oku [a], A. Kubo [a]

[a] *Department of Radiation Oncology, Keio University, Tokyo, Japan*
[b] *Department of Medical Physics and Bioengineering, Christchurch Hospital, Christchurch, New Zealand*
[c] *Department of Radiological Sciences, Ibaraki Prefectural University of Health Sciences, Ibaraki, Japan*

Received 4 July 2007; received in revised form 6 February 2008; accepted 8 February 2008
Available online 18 April 2008

KEYWORDS
Stereotactic radiotherapy;
Lung tumor;
Path-length;
Electron density

Abstract *Purpose:* To clarify the effects of respiratory condition on dose calculation for stereotactic radiotherapy of small lung tumors.
Methods and materials: Computed tomography (CT) data were obtained for nine tumors (diameter, 2.1–3.6 cm; mean, 2.7 cm) during the stable state, deep expiration, and deep inspiration breath-hold states. Rotational irradiation with 3 non-coplanar arcs (Rotational irradiation) and static irradiation with 18 non-coplanar ports (Static irradiation) using 6-MV photons were evaluated using Fast Fourier Transform (FFT) convolution and Multigrid (MG) superposition algorithms. Dose-volume histograms (DVHs), mean path-length (PL) and mean effective path-length (EPL) were calculated.
Results: Although the PL was larger for the inspiration state than for the stable state and the expiration state, the EPL was 0.4–0.5 cm smaller in the inspiration state than in the expiration state ($p = 0.01$ for Rotational irradiation; $p = 0.03$ for Static irradiation). The isocenter dose obtained by the FFT convolution algorithm was 7–12% higher than that obtained with the MG superposition algorithm. A leftward shift of the DVH obtained by MG superposition was noted for the inspiration state compared with the expiration state.
Conclusions: The choice of the proper algorithm is important to accounting for changes in respiration state. Differences in isocenter dose were not large among the respiratory states

* Corresponding author. Department of Radiation Oncology, Keio University, 35 Shinanomachi, Shinjuku, Tokyo 160-8582, Japan. Tel.: +81 3 3353 1211x62531; fax: +81 3 3359 7425.
E-mail address: kunieda-mi@umin.ac.jp (E. Kunieda).

doi:10.1016/j.ejmp.2008.02.002

analyzed. EPL was a little shorter for inspiration than for expiration, although there were larger and reverse trends in path length. A leftward shift of the DVH obtained for the inspiration state when MG superposition was used.

Introduction

Stereotactic radiotherapy (SRT) is currently performed to treat small tumors of the trunk [1,2]. In particular, SRT has gained acceptance as an effective means of treatment for lung tumors [3–5]. However, factors such as the presence of inhomogeneous density within the chest, respiratory motion, and lack of lateral electron equilibrium due to a small radiation field may have an effect on the accuracy of the dose calculation for lung SRT performed with an X-ray computed tomography (CT)-based radiation treatment planning system (RTPS) [5,6].

CT scans for SRT planning for lung tumors are often obtained with deep-inspiration breath hold or other breath-hold techniques. To estimate the mean position and range of tumor motion during respiratory cycles, CT scans during free breathing, called "slow CT," are often used [7–10]. A pair of inhalation and exhalation breath-hold CT scans, and four-dimensional CT [11–13] are able to indicate the range of the tumor motion without the blurring effect caused by slow CT. These techniques were well summarized in a report from the American Association of Physicists in Medicine (AAPM) Task Group 76 [14]. However, based on respiratory conditions, variations in lung densities will cause changes in the mean path-length (PL), mean effective path-length (EPL), and energy distributions in the medium and finally bring about a change the density-scaling factor, which is used to correct the inhomogeneity correction.

This study was designed to clarify the effects of respiratory condition on dose distribution using convolution and superposition algorithms [15,16] in SRT for small lung tumors. To determine the range of variations, we evaluated path-length and effective path-length data under extreme breathing conditions (i.e. deep-expiration, and deep-inspiration breath-hold) as well as stable-state breath-hold conditions. Dose distributions were obtained for rotation and multiple static-port irradiation, based on CT images of patients who were scheduled to undergo lung SRT. Furthermore, we investigated changes in dose distribution in the breathing conditions to determine the degree of influence on the dose calculation using clinical algorithms.

Methods

CT images

A total of 9 lung tumors (diameter range, 2.1–3.6 cm; mean, 2.7 cm) from 9 patients diagnosed with early-stage lung cancer (4 men, 5 women; mean age, 70 years) were evaluated. The cases used for this study were selected from consecutive patients treated with SRT for their lung lesions who agreed to be enrolled in this study. The approximate positions of the lesions are indicated in Fig. 1. CT scanning procedures in three breathing conditions and the use of data for this analysis were approved by the Institutional Review Board. Written informed consent was obtained from each participant prior to the CT scans after the purpose of the study had been fully explained.

Whole lungs including tumors were scanned using a multi-detector row (16 rows) helical CT (MDCT) (Aquilion; Toshiba Medical Systems Co., Ltd., Tokyo, Japan). A stereotactic body frame (Elekta AB, Stockholm, Sweden) was used for patient fixation, As a routine procedure for the planning of stereotactic radiotherapy, a series of breath-hold scans were carried out at approximately the mid-point of inhalation and expiration in the stable respiratory cycle (stable-state breath-hold). A series of slow CT scans during stable respiration for the tumor and the adjacent area was carried out to take the tumor motion into account. In addition, for those patients who agreed to take part in this study on a voluntary basis, two series of CT were performed for the whole lung under deep expiration breath-hold and deep inspiration breath-hold conditions. These three-phase breath-hold CT series were used for the following analysis. The breath-hold CT scans were obtained using 0.5 s/rotation, a helical pitch of 5.5, 2-mm thickness, and 7-mm thickness reconstruction with exposure conditions of 120 kV and 200 mA.

Treatment planning

CT data were transferred to 3D-RTPS (XiO version 2.4.0, CMS Co., St. Louis, Missouri, USA) via DICOM protocol from the CT scanner. CT data for stable-state breath-hold were used for treatment planning of the actual treatment.

Body contours, both lungs, and gross target volume (GTV) were delineated on each of the three-phase CT images by a radiation oncologist. The GTV was first created on stable-state breath-hold CT images and the delineation was then copied manually to the expiration and inspiration breath-hold images to follow the tumor motion. The isocenters were placed at the center of the GTV for each breath-hold CT series. A window width of 1500, and a window level of −700 were used to determine the GTV. Clinical target volume (CTV) was the same as the GTV and a 0.5 cm margin was added to the CTV in all directions in order to create the planning target volume (PTV).

For this experimental study, despite whatever technique was actually used for treatment, we adopted Rotational Irradiation with 3 non-coplanar arcs (−30°, 0°, +30° couch angle; 220° gantry arc on the lesion side) as shown in Fig. 2a (Rotational Irradiation) and Static Irradiation with 18 non-coplanar ports (−30°, 0°, +30° couch angle; 0°, 30°, 150°, 180°, 210°, 330° gantry angle on the lesion side) as shown in Fig. 2b (Static Irradiation). In all cases an additional 0.5 cm field margin was added to the PTV to generate a rectangular field size. Although the PTV sizes were

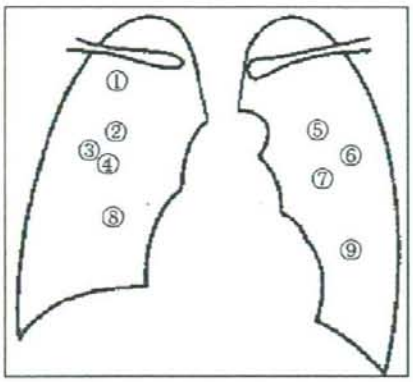

case	location	P-T/A-P
1	Right upper	5.1/12.
2	Right upper	3.0/12.
3	Right upper	5.2/12.
4	Right upper	9.3/16.
5	Left upper	11./14.
6	Left upper	2.0/13.
7	Left upper	7.5/12.
8	Right middle	4.0/17.
9	Left lower	8.6/13.

Figure 1 Locations of the nine lesions evaluated in this study. The table on the right indicates the tumor position in the antero-posterior direction. P-T: distance from the posterior margin of the lung to the center of tumor on an antero-posterior line through the center of the tumor on an axial CT plane that includes the tumor. A-P: distance between the anterior and posterior margin of the lung on the same line.

relatively small, minimal field sizes of 4 cm by 4 cm were employed.

Beams of 6-MV photon generated from the linear accelerator (ML15-MV, Mitsubishi Electric Co., Tokyo, Japan) were used. Dose calculations were carried out to deliver 12 Gy at the isocenter, and the all static beams or arcs were weighted equally at the isocenter. In that condition, the sum of the monitor unit (MU) for all beams required to give 12 Gy at the isocenter was recorded and the doses at the isocenter were rescaled to the doses when 100 MU were used for the total of the dose delivery (i.e. the rescaled isocenter dose = 12 (Gy) × 100 (MU)/ the sum of monitor unit for all beams). Two dose calculation algorithms, the Fast Fourier Transform (FFT) convolution and the multigrid (MG) superposition [17] based on a convolution and a superposition algorithms [15,16], were used.

Path-length and effective path-length

Relative electron density maps were generated from CT data and a calibration curve that had been previously obtained from CT scanning of a calibration phantom. Path-lengths, L, and effective path-lengths, L_{eff} were calculated with pixel-by-pixel integration of values from the relative electron density map through the beam path, from the incident point of the beam center-line to the isocenter at the center of the tumor. Mean path-length, $\bar{L}$ and mean effective path-length, $\bar{L}_{eff}$ for Static Irradiation were calculated from values obtained by various beams, i, according to the following equations:

$$\bar{L} = \sum_{i=1}^{n} L_i / n \qquad (1)$$

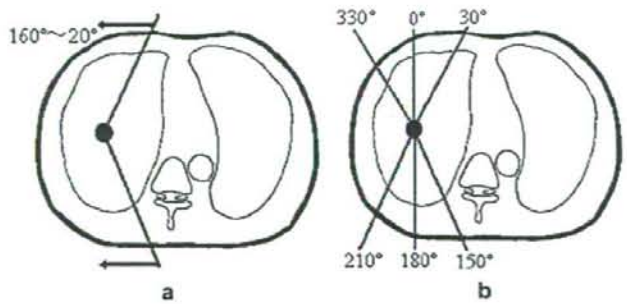

Figure 2 Beam configurations. (a) Rotational Irradiation with three non-coplanar arcs (Rotational Irradiation). For a tumor in the right lung, rotational angles of 220° (from 160° to 20°) for couch angles of 30°, 0° and +30° were applied. For a tumor in the left lung, the arc rotations were diametrically opposite. (b) Static Irradiation with 18 non-coplanar ports (Static Irradiation). Gantry angles of 0°, 30°, 150°, 180°, 210°and 330° for couch angles of −30°, 0° and +30° were used.

$$\bar{L}_{eff} = \sum_{i=1}^{n} L_{eff,i}/n \quad (2)$$

where n is the number of beams.

$\bar{L}$ and $\bar{L}_{eff}$ Rotational Irradiation were obtained from lengths or effective lengths calculated per every 10° rotation.

$$\bar{L} = \frac{1}{m \cdot n} \sum_{i,j=1}^{n,m} L_{i,j} \quad (3)$$

$$\bar{L}_{eff} = \frac{1}{m \cdot n} \sum_{i,j=1}^{n,m} L_{eff,i,j} \quad (4)$$

where n is the number of arcs and m = Rotation Angle/10° for each arc.

Dose volume histogram (DVH)

Dose volume histograms (DVH) of the GTV were calculated for each patient under inspiration and expiration conditions for Rotational Irradiation.

Statistical analysis

The t-test was used to compare values for different respiratory conditions. p-values less than 0.05 were considered statistically significant.

Results

In Fig. 3, examples of dose distribution are presented for Rotational Irradiation and Static Irradiation using serial CT data from inspiration. Table 1 indicates path-length, relative electron density, and effective path-length for three breathing conditions (stable-state, inspiration, and expiration breath-hold) according to the irradiation method. Both the mean path-length and mean effective path-length were larger for Static Irradiation than for Rotational Irradiation. In contrast, relative electron density was lower for the former than for the latter. The largest path-length was obtained with inspiration, followed by stable-state and expiration in that order. The difference in mean path-length between inspiration and expiration was 0.5 cm for Rotational Irradiation and 0.6 cm for Static Irradiation. Relative electron density was lower in inspiration than in expiration. Effective path-length was about 0.4–0.5 cm shorter in inspiration than in expiration.

Table 1 Path-length, effective path-length, and relative electron density measured from CT data in three breathing conditions

		Rotational Irradiation	Static Irradiation
Path-length (cm)	Stable-state	9.4 ± 1.8	10.1 ± 1.2
	Inspiration	9.7 ± 1.9	10.6 ± 1.2
	Expiration	9.2 ± 1.8	9.8 ± 1.3
Effective path-length (cm)	Stable-state	5.7 ± 1.3	5.8 ± 1.2
	Inspiration	5.3 ± 1.3	5.5 ± 1.4
	Expiration	5.8 ± 1.3	5.9 ± 1.3
Relative electron density	Stable-state	0.60	0.57
	Inspiration	0.55	0.52
	Expiration	0.63	0.60

Path-length is given as mean ± SD, effective path-length as mean ± SD, and relative electron density as mean. SD, standard deviation.

P values generated from the t-test were used to assess variation of effective path-length in expiration and inspiration ($p = 0.01$ for Rotational Irradiation, $p = 0.03$ for Static Irradiation, both statistically significant).

Table 2 shows required dose at isocenter for 100 MU which was calculated by the FFT convolution and MG superposition algorithms [17] in all three breathing conditions for both types of irradiation procedures. The dose obtained by the FFT convolution algorithm was 7–12% higher than the dose obtained by the MG superposition algorithm. Fig. 4 shows effective path-length and the isocenter dose per 100 MU for each of the nine lesions. Although the isocenter dose obtained by the FFT convolution algorithm linearly decreased relative to effective path-length, there was variation among cases with the MG superposition algorithm.

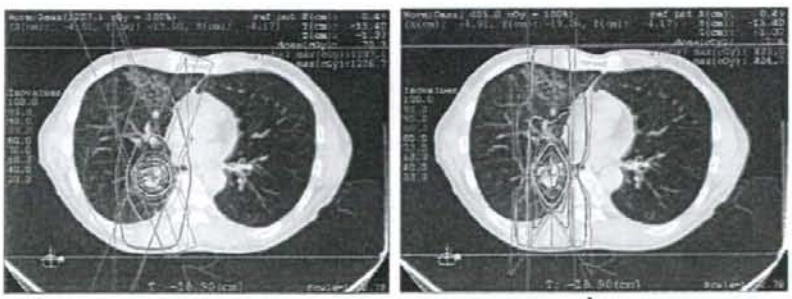

a b

Figure 3 Examples of dose distribution for Rotational Irradiation (a) and Static Irradiation (b).

Table 2 The isocenter dose (Gy) per 100 MU calculated with two calculation algorithms in three breathing conditions

		Rotational Irradiation	Static Irradiation
Convolution (Gy)	Stable-state	0.808	0.799
	Inspiration	0.822	0.809
	Expiration	0.803	0.794
Superposition (Gy)	Stable-state	0.745	0.735
	Inspiration	0.743	0.722
	Expiration	0.750	0.738
Superposition/ convolution (%)	Stable-state	0.922	0.920
	Inspiration	0.904	0.892
	Expiration	0.934	0.929

For each patient, integral DVHs for GTV in inspiration and expiration conditions for Rotational Irradiation were obtained, and all DVHs for each patient were averaged (Fig. 5). Although there were no statistical differences in integral DVH obtained by the FFT convolution algorithm between the inspiration and expiration conditions, with the MG superposition algorithm the difference was pronounced. With the latter algorithm, a leftward shift of the integral DVH was noted in inspiration compared with expiration. D_{95} (the minimal dose delivered to 95% of the target volume) for inspiration, stable-state and expiration conditions were 0.878, 0.91 and 0.912 Gy, respectively. D_{75} for inspiration, stable-state and expiration conditions were 0.891, 0.922 and 0.923 Gy, respectively. There were significant differences between inspiration and stable-state, as well as between expiration and inspiration ($p < 0.05$).

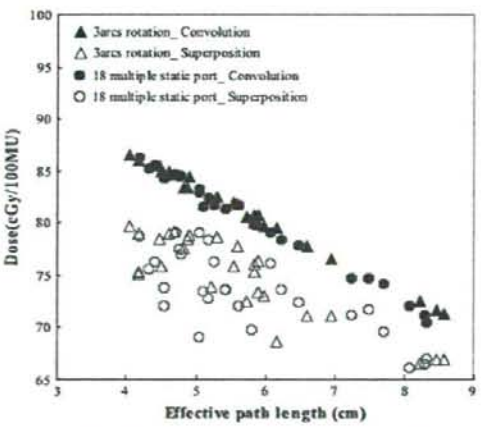

Figure 4 Effective path-length and the isocenter dose calculated by two algorithms (convolution and superposition) plotted for nine tumors in three breathing conditions. Effective path-lengths and the doses were calculated for each static port and averaged. Effective path-lengths and doses for arc irradiations were calculated in the 9 isocenters, each with 3 arcs. The calculations were carried out for each 10° rotation of the gantry and then averaged.

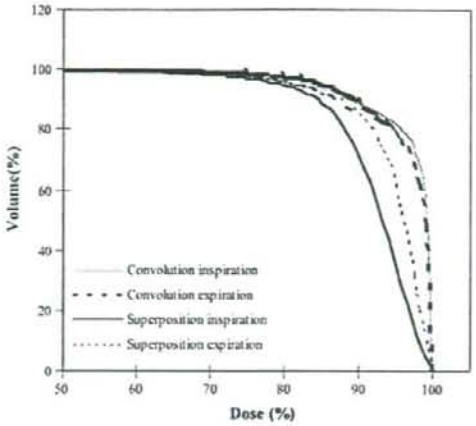

Figure 5 Integral dose-volume histograms (DVHs) for three breathing conditions calculated for Rotational Irradiation with FFT convolution and MG superposition algorithms. DVH curves were obtained for the nine tumors and then averaged.

Discussion

During normal respiration, lung volume typically changes by 20% from 3.3 to 4.1 l on average, as observed in a 10-patient study [18]. However, there are few reports regarding the effect of respiration on the dose distribution of stereotactic radiotherapy for lung tumors.

Our study performed on deep inspiration and expiration conditions indicates that the path-length increased by 2.4–3.7% in stable-state and 5.3–8.7% in inspiration relative to that in the expiration state. Relative electron density decreased by 4.2–4.3% in stable-state and 12.9–13.7% in inspiration relative to expiration.

Although the respiratory conditions were extreme, our results did not indicate large variation in effective path-length under these three respiratory conditions. Obtained effective path-length in inspiration was shorter than that in expiration. These "paradoxical" changes in effective path-length (shorter effective path-length with longer physical path-length) can be easily explained by the expansion of the thoracic cavity with inspiration. However, changes in effective path-length are more complex because the effective path-length is the sum of the product of the path-length in tissue and its electron density. The path-length in the lung increased, whereas electron density decreased, in relation to lung expansion. Our study indicated that the effective path-length decreased in stable-state and inspiration compared with expiration ($p < 0.05$). Observed changes in the path-length, the density and the effective path-length associated with respiratory movement can be expressed as a simplified sphere model.

Expiration and inhalation respiratory lung conditions are expressed with small and large spheres, with the radii of the spherical surfaces representing path-lengths (Fig. 6). Because total lung mass is constant, the relationship between path-length and relative electron density in expiration e and inhalation i is expressed using the following equation:

$$\frac{4}{3}\pi L_e^3 \rho_e = \frac{4}{3}\pi L_i^3 \rho_i \quad (5)$$

where L_e and L_i are the path-length of expiration and inspiration, respectively, and ρ_e and ρ_i are relative electron density of expiration and inhalation, respectively.

Because the effective path-length (L_{eff}) is a product of path-length and relative electron density, Eq. (5) can be expressed as

$$(L_e/L_i)^2 = 1/(L_{eff_e}/L_{eff_i}) \quad (6)$$

In this model, relative electron density is inversely proportional to the path-length cubed. Thus, minute changes in path-length may have a great influence on relative electron density. Moreover, this model indicates the effective path-length is inversely proportional to the square of the path-length. A similar deformity of the lung may occur during the inspiration and expiration. Regarding the human chest, respiration is associated with deformity of the thoracic cavity due to diaphragmatic motion and intercostal muscle constriction where the expansion of the lung and thorax or downward movement of the diaphragm during the inspiration are not isotropic. The involvement of diaphragmatic motion in lung respiration is reportedly greater than costal motion [19,20]. In addition, the changes of in path-length and density are expected to be different depending on the beam orientation.

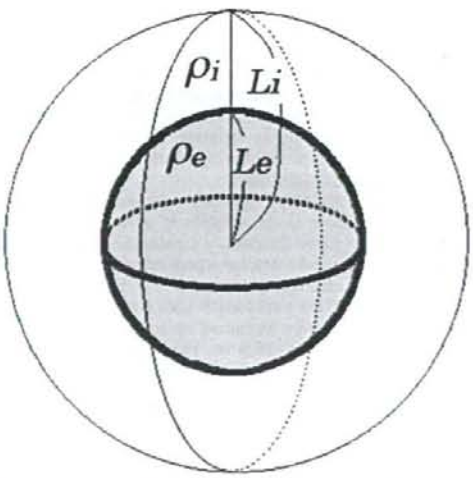

Figure 6 A spherical lung motion model. The inner sphere represents expiration (e) and the outer represents inspiration (i). Radii of the spheres represent path-lengths of expiration and inspiration (L_e, L_i). Relative electron density (ρ_e, ρ_i).

Rotational Irradiation using multiple arcs and Static Irradiation using multiple fields are very common in SRT techniques and selection of the technique depends on the institutional protocols. A comparison of path length, effective path length and relative electron densities between Rotational Irradiation and Static Irradiation for different respiratory conditions are shown in Table 1. Although the effective path lengths for these two irradiation techniques were very similar, there was approximately a 5% difference in electron density between the two techniques. With Rotational Irradiation, longer path-lengths were noted. Interestingly, the impact of these differences on dose/100 MU among different respiratory conditions was negligible (Table 2). However, the isocenter doses per 100 MU delivery were less with the MG superposition calculation than with FFT convolution. The ratios of MG superposition to FFT convolution doses were also indicated in Table 2. The ratios were low in the inspiration phase both with Rotational and Static Irradiation. The lower ratio of MG superposition to FFT convolution doses with inspiration phase can be explained by the difference of the algorithms, as discussed below and the lower lung density in the inspiration phase.

A comparison of the isodose distributions between Rotational Irradiation and Static Irradiation with non-conformal fields is shown in Fig. 3. Rotational Irradiation provides a graphically better dose distribution in this case. However, further optimization of the static fields may yield better results. This requires further investigation.

Three-dimensional (3D) dose distributions are calculated with various algorithms using anatomical data obtained by CT scans. In convolution and superposition algorithms, the dose is computed by convolving the total energy released per unit mass (TERMA) at each point in the patient with the energy deposition kernel [21]. The kernel is generated using the Monte Carlo (MC) particle transport calculation, and it can be divided into the primary and the scatter component [21,22]. In both dose calculation algorithms, the TERMA is computed from fluence, and 3D dose distributions are calculated by separating the energy diffusion process into a primary dose convolution and a scatter dose convolution. Beam attenuation related to the density of the medium is an intrinsic factor to calculate released energy (primary and scatter) associated with the TERMA. Kernel hardening correction factors are computed and applied to the TERMA based on the KERMA (kinetic energy released per unit mass) to TERMA ratio at each depth and at the surface [23,24]. Tissue inhomogeneities cause the greatest distortion of the energy deposition kernels and of the resultant dose distribution compared with those calculated in the water phantom. Therefore, in the MG superposition algorithm, a density scaling method based on O'Connor's theorem [25] is used to scale the kernels by calculating the average density along the straight-line path between the dose deposition and the interaction voxels [17]. However, there are reported differences in the calculated dose of 10% or more among various algorithms [26,27]. Because of the reason mentioned above, the MG superposition algorithm is preferred to FFT convolution, which might result in underdosage of the lung tumor by almost 10% [17,27,28].

In the FFT convolution algorithm, kernels remain invariant over the entire space in which they are applied [17]; therefore, the dose/MU decreases linearly with increasing effective path length, which can be seen in Fig. 4. The MG superposition algorithm, however, shows less of a relationship between dose/MU and effective depth. Small effective depths may require the same dose/MU as much larger effective depths. This can be attributed to the kernels accounting for the 3D variations in electron density in the patient [17], for example the lack of lateral electronic equilibrium.

The DVH for GTV, which was calculated in inspiration, stable-state and expiration conditions for Rotational irradiation, varied depending on the dose calculation algorithm in use. When the MG superposition method was used, a leftward shift of DVH was found in inspiration, in which relative electron density was smaller than that in expiration. The reason for this may be explained from the facts that in the MG superposition algorithm, the density of material between the interaction and dose deposition points is taken into account [17]. For a small lung tumor with different adjacent lung densities, ranges of secondary electrons will be different. Lung density with inspiration will give a longer range of the secondary electrons than with the expiration; therefore, inspiration condition will have a lower electronic equilibrium and dose coverage in the target than the expiration condition.

This study has shown that differences in lung densities in between inspiration and expirations are significant. For small lung tumors the planned dose distributions can change with the breathing phase and the algorithm. In the case of the MG superposition algorithm a better dose homogeneity in the GTV can be achieved when irradiation is done in the expiration phase compared to the inspiration phase, whereas the phase of breathing has very little effect on the planned dose distributions when the FFT convolution algorithm is used. The use of breathing adapted techniques, such as breath-hold or synchronized irradiation, is also important to reduce the planning target volume for stereotactic lung irradiations.

Acknowledgement

We express our gratitude to David McKay, Medical Physicist, Oncology Service, Christchurch Hospital, Christchurch, New Zealand for his kind advice and cooperation in the preparation of this manuscript.

References

[1] Lax I, Blomgren H, Naslund I, Svanstrom R. Stereotactic radiotherapy of malignancies in the abdomen. Methodological aspects. Acta Oncol 1994;33:677–83.

[2] Blomgren H, Lax I, Naslund I, Svanstrom R. Stereotactic high dose fraction radiation therapy of extracranial tumors using an accelerator. Clinical experience of the first thirty-one patients. Acta Oncol 1995;34:861–70.

[3] Nagata Y, Takayama K, Matsuo Y, Norihisa Y, Mizowaki T, Sakamoto T, et al. Clinical outcomes of a phase I/II study of 48 Gy of stereotactic body radiotherapy in 4 fractions for primary lung cancer using a stereotactic body frame. Int J Radiat Oncol Biol Phys 2005;63:1427–31.

[4] Onishi H, Araki T, Shirato H, Nagata Y, Hiraoka M, Gomi K, et al. Stereotactic hypofractionated high-dose irradiation for stage I nonsmall cell lung carcinoma: clinical outcomes in 245 subjects in a Japanese multiinstitutional study. Cancer 2004;101:1623–31.

[5] Haedinger U, Krieger T, Flentje M, Wulf J. Influence of calculation model on dose distribution in stereotactic radiotherapy for pulmonary targets. Int J Radiat Oncol Biol Phys 2005;61: 239–49.

[6] Saitoh H, Fujisaki T, Sakai R, Kunieda E. Dose distribution of narrow beam irradiation for small lung tumor. Int J Radiat Oncol Biol Phys 2002;53:1380–7.

[7] Takeda A, Kunieda E, Shigematsu N, Hossain DM, Kawase T, Ohashi T, et al. Small lung tumors: long-scan-time CT for planning of hypofractionated stereotactic radiation therapy—initial findings. Radiology 2005;237:295–300.

[8] Lagerwaard FJ, Van Sornsen de Koste JR, Nijssen-Visser MR, Schuchhard-Schipper RH, Oei SS, Munne A, et al. Multiple "slow" CT scans for incorporating lung tumor mobility in radiotherapy planning. Int J Radiat Oncol Biol Phys 2001;51: 932–7.

[9] van Sornsen de Koste JR, Lagerwaard FJ, Nijssen-Visser MR, Graveland WJ, Senan S. Tumor location cannot predict the mobility of lung tumors: a 3D analysis of data generated from multiple CT scans. Int J Radiat Oncol Biol Phys 2003;56: 348–54.

[10] de Koste JR, Lagerwaard FJ, de Boer HC, Nijssen-Visser MR, Senan S. Are multiple CT scans required for planning curative radiotherapy in lung tumors of the lower lobe? Int J Radiat Oncol Biol Phys 2003;55:1394–9.

[11] Starkschall G, Forster KM, Kitamura K, Cardenas A, Tucker SL, Stevens CW. Correlation of gross tumor volume excursion with potential benefits of respiratory gating. Int J Radiat Oncol Biol Phys 2004;60:1291–7.

[12] Underberg RW, Lagerwaard FJ, Slotman BJ, Cuijpers JP, Senan S. Use of maximum intensity projections (MIP) for target volume generation in 4DCT scans for lung cancer. Int J Radiat Oncol Biol Phys 2005;63:253–60.

[13] Underberg RW, Lagerwaard FJ, Cuijpers JP, Slotman BJ, van Sornsen de Koste JR, Senan S. Four-dimensional CT scans for treatment planning in stereotactic radiotherapy for stage I lung cancer. Int J Radiat Oncol Biol Phys 2004;60: 1283–90.

[14] Keall PJ, Mageras GS, Balter JM, Emery RS, Forster KM, Jiang SB, et al. The management of respiratory motion in radiation oncology report of AAPM Task Group 76. Med Phys 2006;33:3874–900.

[15] Mackie TR, Scrimger JW, Battista JJ. A convolution method of calculating dose for 15-MV x rays. Med Phys 1985;12:188–96.

[16] Ahnesjo A. Collapsed cone convolution of radiant energy for photon dose calculation in heterogeneous media. Med Phys 1989;16:577–92.

[17] Miften M, Wiesmeyer M, Monthofer S, Krippner K. Implementation of FFT convolution and multigrid superposition models in the FOCUS RTP system. Phys Med Biol 2000;45:817–33.

[18] Biancia CD, Yorke E, Chui CS, Giraud P, Rosenzweig K, Amols H, et al. Comparison of end normal inspiration and expiration for gated intensity modulated radiation therapy (IMRT) of lung cancer. Radiother Oncol 2005;75:149–56.

[19] Walsh JM, Webber Jr CL, Fahey PJ, Sharp JT. Structural change of the thorax in chronic obstructive pulmonary disease. J Appl Physiol 1992;72:1270–8.

[20] Krayer S, Rehder K, Vettermann J, Didier EP, Ritman EL. Position and motion of the human diaphragm during anesthesia-paralysis. Anesthesiology 1989;70:891–8.

[21] Mackie TR, Bielajew AF, Rogers DW, Battista JJ. Generation of photon energy deposition kernels using the EGS Monte Carlo code. Phys Med Biol 1988;33:1–20.

[22] Boyer AL. Relationship between attenuation coefficients and dose-spread kernels. Radiat Res 1988;113:235–42.
[23] Hoban PW, Murray DC, Round WH. Photon beam convolution using polyenergetic energy deposition kernels. Phys Med Biol 1994;39:669–85.
[24] Hoban PW. Accounting for the variation in collision kerma-to-terma ratio in polyenergetic photon beam convolution. Med Phys 1995;22:2035–44.
[25] O'Connor JE. The variation of scattered x-rays with density in an irradiated body. Phys Med Biol 1957;1:352–69.
[26] Engelsman M, Damen EM, Koken PW, van't Veld AA, van Ingen KM, Mijnheer BJ. Impact of simple tissue inhomogeneity correction algorithms on conformal radiotherapy of lung tumours. Radiother Oncol 2001;60:299–309.
[27 Nishio T, Kunieda E, Shirato H, Ishikura S, Onishi H, Tateoka K, et al. Dosimetric verification in participating institutions in a stereotactic body radiotherapy trial for stage I non-small cell lung cancer: Japan Clinical Oncology Group trial (JCOG0403). Phys Med Biol 2006 Nov 7;51(21):5409–17. [Epub 2006 Oct 6].
[28] Miften M, Wiesmeyer M, Kapur A, Ma CM. Comparison of RTP dose distributions in heterogeneous phantoms with the BEAM Monte Carlo simulation system. J Appl Clin Med Phys/Am Coll Med Phys 2001;2:21–31.

Radiotherapy and Oncology 86 (2008) 258–263
www.thegreenjournal.com

Postal dosimetry

Feasibility study of glass dosimeter postal dosimetry audit of high-energy radiotherapy photon beams

Hideyuki Mizuno[a,*], Tatsuaki Kanai[a], Yohsuke Kusano[b], Susumu Ko[a], Mari Ono[c], Akifumi Fukumura[a], Kyoko Abe[d], Kanae Nishizawa[a], Munefumi Shimbo[e], Suoh Sakata[f], Satoshi Ishikura[g], Hiroshi Ikeda[g]

[a]*Research Center for Charged Particle Therapy, National Institute of Radiological Sciences, Chiba, Japan,* [b]*Accelerator Engineering Corporation, Chiba, Japan,* [c]*Keio University Hospital, Tokyo, Japan,* [d]*Toho University Graduate School, Funabashi, Japan,* [e]*Saitama Medical Center, Kawagoe, Japan,* [f]*Association for Nuclear Technology in Medicine, Tokyo, Japan,* [g]*National Cancer Center, Tokyo, Japan*

Author

***Introduction*: The characteristics of a glass dosimeter were investigated for its potential use as a tool for postal dose audits. Reproducibility, energy dependence, field size and depth dependence were compared to those of a thermoluminescence dosimeter (TLD), which has been the major tool for postal dose audits worldwide.**

***Materials and methods*: A glass dosimeter, GD-302M (Asahi Techno Glass Co.) and a TLD, TLD-100 chip (Harshaw Co.) were irradiated with γ-rays from a ^{60}Co unit and X-rays from a medical linear accelerator (4, 6, 10 and 20 MV).**

***Results*: The dosimetric characteristics of the glass dosimeter were almost equivalent to those of the TLD, in terms of utility for dosimetry under the reference condition, which is a 10×10 cm^2 field and 10 cm depth. Because of its reduced fading, compared to the TLD, and easy quality control with the ID number, the glass dosimeter proved to be a suitable tool for postal dose audits. Then, we conducted postal dose surveys of over 100 facilities and got good agreement, with a standard deviation of about 1.3%.**

***Conclusions*: Based on this study, postal dose audits throughout Japan will be carried out using a glass dosimeter.**
 Radiotherapy and Oncology 86 (2008) 258–263.

Keywords: Postal dose audit; Glass dosimeter; Reference condition

Thermoluminescence dosimeters (TLD) have been used as the standard tool for dose audits for the past few decades [1,5,9,10]. They have good reproducibility and small energy dependence [12,13]. However, TLD powder requires careful handling and fading correction. On the other hand, glass dosimeters are almost free from the fading effect and can be read repeatedly [15]. They have been used for personal radiation monitoring for a long time. However, the problems of its high pre-dose and energy dependence prevented this tool from becoming an alternative to TLD [15]. Recently, a new type of glass rod dosimeter has become commercially available, which achieves great improvement in the reading method to avoid pre-dose effect [4]. Tsuda [17] reported its reproducibility as 0.82% in the coefficient of variance, which is comparable that of to TLD. Furthermore, good linearity, up to 10 Gy, and less fading, 1.90% after 129 days, were also achieved. Araki et al. [2] used a glass dosimeter to measure the Gamma-Knife helmet output factors and gave an indication of its superiority over TLD. They [3] also applied the glass dosimeter to linac beams of several energies and achieved slight energy dependencies within 2%. The glass dosimeter's energy dependence is not a serious impediment to dosimetry under reference conditions.

Regarding the audit system, IAEA/WHO, the Radiological Physics Center (RPC) and the European Society for Therapeutic Radiology and Oncology (ESTRO) have performed postal dose audits worldwide or nationwide [1,5,6,9–11]. However, Japan has not yet been included in any audit group. In Japan, only a few pilot studies have been done [7]. Shimbo et al. [16] developed the postal dose audit system using a glass dosimeter. We are now on a project to establish a permanent dose audit system based on their system. Glass dosimeters have the potential to become the next generation of detectors for the audit system because of their handling advantage, reduced fading (relative to TLD) and repeatable readout. In this article, we report the comparison between a glass dosimeter and TLD as the tool for postal audits, focusing on its application to reference condition dosimetry. In addition, the results of the pilot postal audit study are shown, which was conducted at over 100 radiotherapy facilities.

0167-8140/$ - see front matter doi:10.1016/j.radonc.2007.10.024

Materials

Glass dosimeter

The glass dosimeter (DOSE ACE, Asahi Techno Glass Corporation; ATG) is silver-activated phosphate glass. Its weight composition is as follows: 11.0% Na, 31.55% P, 51.16% O, 6.12% Al and 0.17% Ag [17]. Though it is not the tissue-equivalent material, it does not affect our application such as relative dosimetry between our standard dose and the dose of certain hospital. Its dimensions are 1.5 mm in diameter and 12 mm in length. ID number is engraved for each element. It is based on radiophotoluminescence (RPL). Radiations produce RPL centers, which emit orange luminescence by UV-ray excitation. After emitting the luminescence, they will return to the stable RPL centers. Therefore, the numbers of RPL centers stay constant, allowing infinite numbers of readings for the same irradiation. In this study, outputs of glass dosimeters were average of five times sequential reading. The RPL centers are cleared by annealing (400 °C with 30 min), so that we can use the element sequentially. An FDG-1000 (ATG) was used as a reader.

The major dosimetric features taken into account were reproducibility and energy dependence. The reproducibility of the RPL signal depends on the element's cutting precision and UV-ray output stability. As for energy dependence, the mass energy absorption coefficient of the glass dosimeter, silver-activated metaphosphate, is several times higher than that of TLD, LiF, for low energy photons around 25 keV (see Fig. 1). This can affect the energy dependence factor.

Thermoluminescent dosimeter

The thermoluminescent dosimeter (TLD-100, Harshaw) is lithium fluoride doped with magnesium and titanium. Several forms are provided such as powders, chips, rods and cubes. Absorbed energy is stored in the crystal lattice, which results in visible light emission by heating. Because of its good physical aspects, including size, tissue-equivalent composition and fine reproducibility, the TLD-100 has been widely used as a postal dose audit tool. We used a chip type with a size of 3.2 mm × 3.2 mm × 0.9 mm. The reader was a Harshaw 5500. The reading temperature is from 50 to 400 °C in order to accumulate the main peak (~210 °C) of glow curve. Annealing was done by the combination of 400 °C for 1 h and 100 °C for 2 h.

Tough water phantom

A water equivalent solid phantom, called the tough water phantom (Kyoto Kagaku Co.), was used. It consists mainly of C, O and H. Its density, mean atomic number and electron density are 1.01 g/cm^3, 7.42 and 3.25×10^{23}/cm^3, respectively. Those of water are 1.00 g/cm^3, 7.42 and 3.34×10^{23}/cm^3, respectively. Its size was 30 cm × 30 cm, it was a slab type and its central region was gouged to contain the glass dosimeters and TLDs.

Investigation of dosimetric characteristics

Experiments

Reproducibility

Reproducibility was examined for both dosimeters, glass dosimeter and TLD, using ^{60}Co γ-rays (Yoshizawa-LA, TYC-3001) and linac X-rays (Varian, Clinac21EX; 6 MV, 10 MV). Dosimeters were set at a reference depth of 10 cm in the tough water phantom (Fig. 2). Field size was 16 cm ϕ for ^{60}Co γ-rays and 10 × 10 cm^2 for X-rays. For each beam, 15 elements were irradiated uniformly. Each element's output was corrected with its own sensitivity. Corrected outputs were divided by the average of 15 elements' output. The measurement cycle, from irradiation to annealing, was done three times to decrease the statistical error.

Energy dependence of glass dosimeter

Energy dependence was examined for the glass dosimeter using ^{60}Co γ-rays and linac X-rays (Mitsubishi, EXL-15DP; 4 MV, Varian, Clinac21EX; 6 MV, 10 MV and Clinac23EX; 20 MV). The experimental setup was the same as in Fig. 2, and the measurements using the ionization chamber were taken under the same conditions. The stability of the output of ^{60}Co γ-rays or linac X-rays was much less than 1%. Measurements were done several times to decrease the statistical error. For each measurement, at least 10 elements were used for one energy.

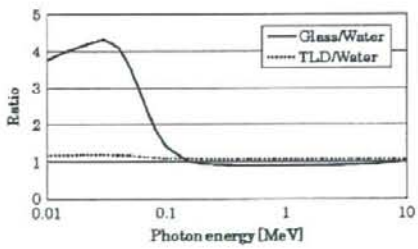

Fig. 1. The ratio of mass energy absorption coefficient between glass dosimeter (silver-activated metaphosphate)/TLD (LiF) and water (acquired from NIST database [14]).

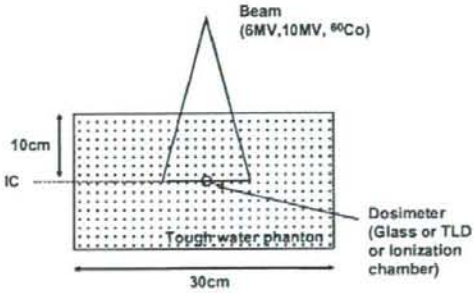

Fig. 2. Setup of reproducibility and energy dependence experiments; dosimeters were placed at 10 cm depth in the isocenter (IC).

The protocol used to determine the absolute dose was the Japanese code, Standard Dosimetry of Absorbed Dose in External Beam Radiotherapy (Standard Dosimetry 01), which is based mainly on IAEA Technical Reports Series No. 398.

Field size and depth dependence

To examine the glass dosimeter's response to low energy photons, field size and depth were changed, because the mean beam energy fell with increasing field size and decreasing depth. Both dosimeters, glass dosimeter and TLD, were irradiated using linac X-rays (Varian, Clinac21EX; 6 MV, 10 MV). Measurements were done at 5×5, 10×10 and 20×20 cm^2 field sizes and at the D_{max} (1.5 cm for 6 MV and 2.5 cm for 10 MV), 5, 10 and 20 cm depth in the tough water phantom. For each condition, 5 elements of glass dosimeter and 3 elements of TLD were used. Once again, the measurements using the ionization chamber were also done under the same condition, that is, measured in tough water phantom.

Results and discussion

Reproducibility

The deviations obtained from both the TLD and the glass dosimeter are shown in Fig. 3. The standard deviation was 0.8% for the glass dosimeter. This value is comparable to the TLD value, 0.7%.

Energy dependence of glass dosimeter

The obtained energy correction factor is shown in Table 1. They were represented as

$$E_q = \frac{\text{Glass(Co)}/D_{med}(\text{Co})}{\text{Glass}(q)/D_{med}(q)}$$

where Glass(Co)/D_{med}(Co) is the light output per unit dose in a medium for ^{60}Co γ-rays. Glass(q)/D_{med}(q) is the light output per unit dose in the same medium for the beam quality q of interest. Beam quality q is represented as $TPR_{20,10}$. The glass dosimeter had a slightly positive correlation with beam energy. However, for the mega-voltage region, the

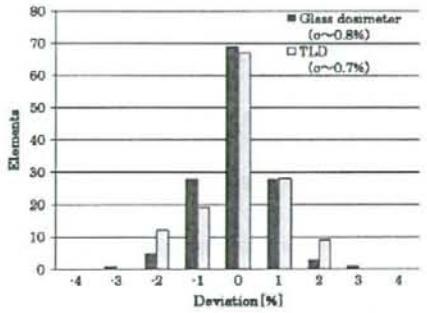

Fig. 3. Reproducibility of glass dosimeter and TLD; 45 elements were repeatedly irradiated by ^{60}Co, 6 and 10 MV X-rays.

Table 1
Quality dependence of glass dosimeter in photon beams by experiment

Energy (MV)	$TPR_{20,10}$	Glass dosimeter factor (E_q)	TLD factor (IPSM 1990, [7,10])
^{60}Co γ-rays	0.58	1.000	1.000
4	0.624	1.007 ± 0.005	
6	0.669	1.014 ± 0.009	1.011
10	0.740	1.026 ± 0.007	1.023
20	0.791	1.029 ± 0.004	

levels of dependence were equivalent to those of the TLD achieved by IPSM [8,13] within the experimental errors. Their TLD factor was obtained by exchanging the glass dosimeter output to the TLD output of above equation.

Field size and depth dependence

The obtained ratios of readings from the glass dosimeter/TLD to ionization chamber outputs are shown in Fig. 4. The values were normalized at reference conditions, 10×10 cm^2 field and 10 cm depth. The ratios for the glass dosimeter were from 0.975 to 1.011 (mean 0.995) for 6 MV, and from 0.973 to 1.031 (mean 0.999) for 10 MV. Those for TLD were from 0.971 to 1.018 (mean 0.996) for 6 MV and from 0.985 to 1.038 (mean 1.014) for 10 MV.

The outputs of the glass dosimeter became slightly smaller, from 1.7 to 2.7%, for a 5×5 cm^2 field compared to 10×10 cm^2 and 20×20 cm^2 fields. This might have been caused by the change in energy spectrum. The mean energy of X-rays becomes higher in the smaller field because of the decrease in scattered photons within the field. However, overall, it seems that the ratios of the glass dosimeter were almost at the same level, or were rather stable, compared to the TLD, for changes in both field size and depth.

Discussion for the dosimetric properties

Even for non-reference dosimetry, glass dosimeter proved to be a potential alternative to TLD. Moreover, the glass dosimeter has the advantage of less fading. In the postal dose audit process, control elements are used to calibrate the reader. Known doses are irradiated onto the control elements by the audit director. Some audit groups irradiate the control elements at only the same timing as the intended facility's irradiation, to minimize the fading effect. By using glass dosimeter, this kind of limitation regarding fading becomes more flexible.

Postal dose audit trial

We conducted a pilot postal audit at over 100 radiation therapy facilities to verify the overall feasibility of establishing a postal dose audit system using glass dosimeters.

Postal tools

We sent 20 glass elements and one set of solid phantoms to participating facilities. The glass dosimeters were contained in tough water phantom (Fig. 5).

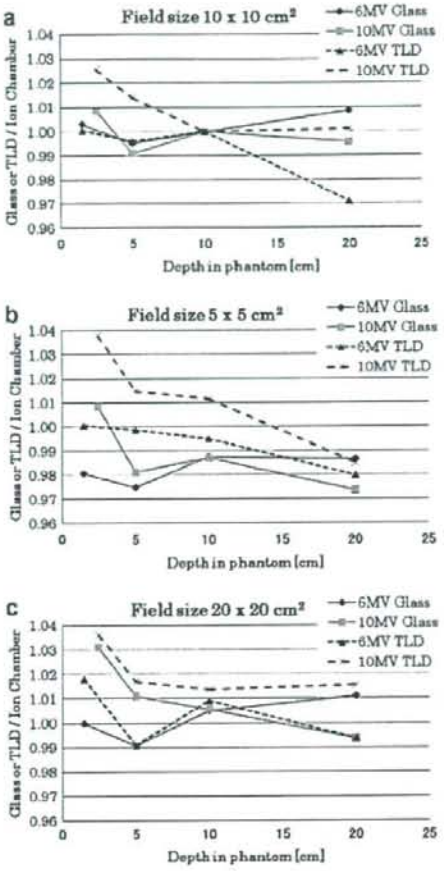

Fig. 4. Ratios between glass dosimeter/TLD and ionization chamber outputs for different field sizes and depths. The field sizes were (a) 10×10 cm^2, (b) 5×5 cm^2, (c) 20×20 cm^2, respectively. The values were normalized at reference conditions, 10×10 cm^2 field and 10 cm depth. The uncertainties of each measured value were 1.5% in standard deviation for glass dosimeter and 1.6% for TLD.

The assignments for the 20 glass elements are shown in Table 2. Twelve elements were "audit elements" that were irradiated with X-rays by a participant (six elements for each of two X-ray energies), six elements were "control elements" that were irradiated with a ^{60}Co beam at NIRS, and two elements were "background elements" that were not irradiated during the audit process. "Control elements" were used to calibrate the reader's sensitivity. These assignments were adopted to minimize the statistical error in final reading outputs under the limitation of the number of sequential readings, 20 elements for one reading run.

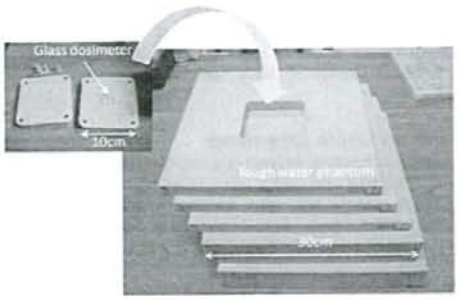

Fig. 5. Glass dosimeter and tough water phantom; tough water phantom is gouged to contain the glass dosimeters.

Table 2
Assignment of one set of glass dosimeters (20 elements)

Name	Element ID	Irradiation condition
Audit elements	Nos. 1–6	1 Gy is irradiated by applied facility by energy 1
	Nos. 7–12	1 Gy is irradiated by applied facility by energy 2
Control elements	Nos. 13–18	1 Gy is irradiated by NIRS by ^{60}Co
Background elements	Nos. 19 & 20	No irradiation

Determination of absorbed dose

The method this audit used to derive the output of irradiation dose to the glass dosimeters is shown below.

1. Twenty elements were read (one run).
2. We repeated the run five times. The rotation or position shifts of the element set in the reader were checked before each run.
3. Outputs of five runs were averaged for each element.
4. We multiplied by the following correction factors (definitions are shown later)
   - Elements' sensitivity correction factor
   - Energy correction factor
   - Phantom correction factor.
5. We averaged the six elements irradiated at the same energy.
6. We determined the calibration ratio between the output of the glass dosimeter and the ionization chamber from the ^{60}Co irradiated data.
7. We multiplied the calibration ratio by the audited elements' output.

The applied facility's final output was defined as in the following equation.

$$D = \sum_{i=1}^{6}(X_i \times I_i) \times E_q \times P_q \times \frac{\mathrm{Dose}_{^{60}\mathrm{Co}}}{\sum_{i=13}^{18}(X_i \times I_i)}$$

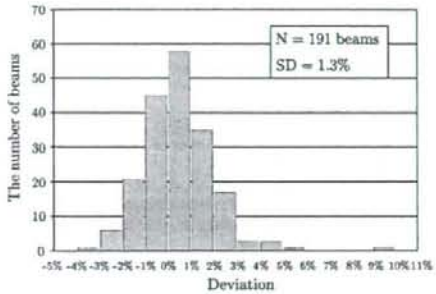

Fig. 6. The result of the postal dose audit for the 191 beams from 4 to 20 MV.

Table 3
Results of first and second postal dose audits

Facility	Beam quality (MV)	Deviation of audit		Probable causes
		First (%)	Second (%)	
A	4	4.1	1.9	Miscalculation of monitor unit
	10	9.2	0.9	(excluded daily MU calibration factor)
B	4	5.7	2.8	Mistake in measurement setup
	10	4.7	3.4	Mistake in calibration factor Substantial change in barometric pressure Uncalibrated thermobarometer
C	4	4.6	2.0	Unclear
	6	2.6	2.1	(Energy switching operation error?)

X_i is the raw output value of the glass element whose ID number is i, I_i is sensitivity correction factor of the glass element whose ID number is i (derived by uniform irradiation using ^{60}Co γ-rays).

$$I_i = \frac{D_{60_{Co}}}{X_i}$$

E_q is the energy correction factor of beam quality "q" (glass elements were irradiated by ^{60}Co γ-rays and 4, 6 and 10 MV X-rays. Correction factor was derived by using the output of the ionization chamber (IC), $D(^{60}\mathrm{Co})$ and $D(q)$, which were measured at the same setup as the glass dosimeter).

$$E_q = \left[\frac{\sum_i X_i(^{60}\mathrm{Co}) \times I_i}{\sum_i X_i(q) \times I_i}\right]^{\mathrm{Glass}} \times \left[\frac{D(q)}{D(^{60}\mathrm{Co})}\right]^{\mathrm{IC}}$$

P_q is the phantom correction factor of beam quality "q."

$$P_q = \frac{D_w}{D_T}$$

D_w is the output of the ionization chamber irradiated by X-rays of beam quality "q" in 10 cm deep water, D_T is the output of the ionization chamber irradiated by X-rays of beam quality "q" 10 cm deep in the tough water phantom, $\mathrm{Dose}_{60_{Co}}$ is the output of the ionization chamber irradiated by ^{60}Co γ-rays just before the irradiation of control elements (ID Nos. 13–18) with same setup.

I_i was assigned to each element to increase the outputs' precision. Of course, I_i, E_q and P_q were determined before the audit trial started. Accumulated uncertainty of each parameter was estimated to be 1.6% in one standard deviation.

Results of postal dose audit trial

We conducted the postal dose audit at 106 facilities using 191 beams. Seventy-seven beams were 4 MV, 31 beams were 6 MV, 81 beams were 10 MV, 1 beam was 14 MV and 1 beam was 20 MV. Fig. 6 shows the overall results of the outputs. The central value was 0.3% and standard deviation was 1.3%; 182 beams (95%) were within ±3%.

One facility showed a big deviation of over 9%. A second postal audit was conducted there, followed by an immediate hearing by phone. Finally, the apparent discrepancy was proved to arise from a participant's miscalculation of a monitor unit (excluding the correction factor of daily monitor chamber response). The result of the second postal audit at that facility was within 2%. Two other facilities, which showed deviations of more than 4%, also underwent a second postal audit. Those results are illustrated in Table 3. Clearly, the results were improved by the second audit, which showed the importance of external audits.

According to the ESTRO/EQUAL postal audit system [5], the optimum level is within ±3%, tolerance level is within ±5% and emergency level is over ±10% deviation. We followed these criteria to report the results to each facility. From this point of view, the reference dose is properly managed by these participants. In addition, glass dosimeters proved to be a suitable tool for postal dose audits.

Conclusion

The dosimetric features of glass dosimeters were examined and compared to those of TLD as tools for postal dose audits. Reproducibility and energy dependence were the same as in the TLD. Additionally, field size and depth dependence were at the same level, and were rather stable. Regarding handling advantages, repeatable readings and low fading, the glass dosimeter is likely to be a suitable tool for postal dose audits. Based on these results, and to check the overall system, we conducted a pilot postal audit at radiotherapy facilities. We got excellent results, in that the central value of the deviation was 0.3% and the standard deviation was 1.3%. A permanent postal dose audit system using glass dosimeters is therefore about to begin in Japan.

Acknowledgments

The postal audit was partially supported by a grant from the Ministry of Health, Labour and Welfare in Japan. The authors express

their thanks to the staff of the NIRS and AEC for their support of glass dosimeter irradiation and reading.

* **Corresponding author. Hideyuki Mizuno**, Research Center for Charged Particle Therapy, National Institute of Radiological Sciences, 4-9-1 Anagawa, Inage-ku, Chiba 263-8555, Japan. *E-mail address:* h_mizuno@nirs.go.jp

Received 16 August 2007; received in revised form 16 October 2007; accepted 17 October 2007; Available online 26 November 2007

References

[1] Aguirre JF, Tailor R, Ibbott G, Stovall M, Hanson, W. Thermoluminescence dosimetry as a tool for the remote verification of output for radiotherapy beams: 25 years of experience. In: Proceedings of the international symposium on standards and codes of practice in medical radiation dosimetry IAEA-CN-96/82. Vienna: IAEA; 2002. p. 191–99.

[2] Araki F, Ikegami T, Ishidoya T, Kubo HD. Measurements of Gamma-Knife helmet output factors using a radiophotoluminescent glass rod dosimeter and a diode detector. Med Phys 2003;30:1976–81.

[3] Araki F, Moribe N, Shimonobou T, Yamashita Y. Dosimetric properties of radiophotoluminescent glass rod detector in high-energy photon beams from linear accelerator and Cyber-Knife. Med Phys 2004;31:1980–6.

[4] Asahi Techno Glass Corporation. Explanation material of RPL glass dosimeter: small element System, Tokyo, Japan; 2000.

[5] Ferreira IH, Dutreix A, Bridier A, Chavaudra J, Svensson H. The ESTRO-QUALity assurance network (EQUAL). Radiother Oncol 2000;55:273–84.

[6] Kroutiliková D, Novotný J, Judas L. Thermoluminescent dosimeters (TLD) quality assurance network in the Czech Republic. Radiother Oncol 2003;66:235–44 .

[7] Hayami A, Inoue T, Kawagoe Y, Fuchihata H. Mailed TLD dose intercomparison at a reference point of high energy photon beams among 11 institutions in Japan. J Jpn Soc Ther Radiol Oncol 1997;9:139–45.

[8] Institute of Physical Science in Medicine (IPSM). Code of practice for high-energy photon therapy dosimetry based on the NPL absorbed dose calibration service. Phys Med Biol 1990;35:1355–60.

[9] Izewska J, Andreo P. The IAEA/WHO TLD postal programme for radiotherapy hospitals. Radiother Oncol 2000;54:65–72.

[10] Izewska J, Andreo P, Vatnitsky S, Shortt KR. The IAEA/WHO TLD postal dose quality audits for radiotherapy: a perspective of dosimetry practices at hospitals in developing countries. Radiother Oncol 2003;69:91–7.

[11] Izewska J, Georg D, Bera P, Thwaites D, Arib M, Saravi M, et al. A methodology for TLD postal dosimetry audit of high-energy radiotherapy photon beams in non-reference conditions. Radiother Oncol 2007;84:67–74.

[12] Kirby TH, Hanson WF, Johnston DA. Uncertainty analysis of absorbed dose calculations from thermoluminescence dosimeters. Med Phys 1992;19:1427–33.

[13] Mobit PN, Mayles P, Nahum AE. The quality dependence of LiF TLD in megavoltage photon beams: Monte Carlo simulation and experiments. Phys Med Biol 1996;41:387–98.

[14] National Institute of Standards and Technology (NIST). Tables of X-ray mass attenuation coefficients and mass energy-absorption coefficients from 1 keV to 20 MeV for elements $Z = 1$ to 92 and 48 additional substances of dosimetric interest. NISTIR 5632 (Version 1.4); 2004.

[15] Piesch E, Burgkhardt B, Vilgis M. Photoluminescence dosimetry: progress and present state of art. Radiat Prot Dosim 1990;33:215–26.

[16] Shimbo M, Nishio T, Ooyama M, et al. Report of the off-site dosimetry. Jpn J Med Phys 2003;23:25–6.

[17] Tsuda M. A few remarks on photoluminescence dosimetry with high energy X-rays. Jpn J Med 2000;20:131–9.

Jpn J Clin Oncol 2008;38(11)723–729
doi:10.1093/jjco/hyn112

Review Article

Quality Assurance of Radiotherapy in Cancer Treatment: Toward Improvement of Patient Safety and Quality of Care

Satoshi Ishikura

Outreach Radiation Oncology and Physics, Clinical Trials and Practice Support Division, Center for Cancer Control and Information Services, National Cancer Center, Chuo-ku, Tokyo, Japan

Received August 29, 2008; accepted September 18, 2008

The process of radiotherapy (RT) is complex and involves understanding of the principles of medical physics, radiobiology, radiation safety, dosimetry, radiation treatment planning, simulation and interaction of radiation with other treatment modalities. Each step in the integrated process of RT needs quality control and quality assurance (QA) to prevent errors and to give high confidence that patients will receive the prescribed treatment correctly. Recent advances in RT, including intensity-modulated and image-guided RT, focus on the need for a systematic RTQA program that balances patient safety and quality with available resources. It is necessary to develop more formal error mitigation and process analysis methods, such as failure mode and effect analysis, to focus available QA resources optimally on process components. External audit programs are also effective. The International Atomic Energy Agency has operated both an on-site and off-site postal dosimetry audit to improve practice and to assure the dose from RT equipment. Several countries have adopted a similar approach for national clinical auditing. In addition, clinical trial QA has a significant role in enhancing the quality of care. The Advanced Technology Consortium has pioneered the development of an infrastructure and QA method for advanced technology clinical trials, including credentialing and individual case review. These activities have an impact not only on the treatment received by patients enrolled in clinical trials, but also on the quality of treatment administered to all patients treated in each institution, and have been adopted globally; by the USA, Europe and Japan also.

Key words: radiation therapy – quality assurance – radiation dosimetry – clinical audit – clinical trials

INTRODUCTION

Radiotherapy (RT) is one of the major options in cancer treatment. As a multimodality treatment combined with surgery and/or chemotherapy, it plays an important role in curing cancers. RT is also a very effective treatment option for palliation and symptom control in advanced or recurrent cancers. In Japan, only a quarter of patients receive RT (1,2), but 52% of patients should receive RT at least once during their treatment of cancer according to the best available evidence (3).

The process of RT is complex and involves understanding of the principles of medical physics, radiobiology, radiation safety, dosimetry, RT planning, simulation and interaction of RT with other treatment modalities. The professional team for RT includes radiation oncologists, medical physicists, radiation technologists and radiation nurses. These professionals work through an integrated process to plan and deliver RT to cancer patients. The sequential process is shown in Fig. 1 and each step needs quality control (QC) and quality assurance (QA) to prevent errors and to give high confidence that patients will receive the prescribed treatment correctly (4).

For reprints and all correspondence: Satoshi Ishikura, Outreach Radiation Oncology and Physics, Clinical Trials and Practice Support Division, Center for Cancer Control and Information Services, National Cancer Center, 5-1-1 Tsukiji, Chuo-ku, Tokyo 104-0045, Japan. E-mail: sishikur@ncc.go.jp

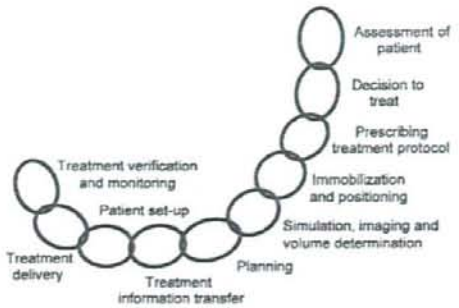

Figure 1. Sequential process of planning and delivering radiotherapy to patients.

The current paradigm of quality management (QM) in RT focuses on measuring the functional performance of RT equipment by measurable parameters with tolerances set at strict but achievable values. Guidelines for these have been provided by: the American Association of Physicists in Medicine (AAPM) in various documents, such as Task Group (TG) 40, 43, 53, 56, 59, 60 and 64 (5–11); the American College of Radiology and the American College of Medical Physics in reports on RTQA; the European Society for Therapeutic Radiology and Oncology (ESTRO) in a report on RTQA (12); the International Electrotechnical Commission publications on functional performance of RT equipment; and the International Organization for Standardization (ISO). The Japanese Society for Therapeutic Radiology and Oncology has also published guidelines in accordance with these for domestic RT institutions. Most of these reports recommend that every parameter that can be checked should be checked. This approach does not provide guidelines for optimally distributing resources for QA and QM activities to maximize the quality of patient care. This is a major problem, because almost no facility has the personnel to cover everything. The difficulty of this situation worsens as new advanced technologies, such as intensity-modulated radiation therapy (IMRT) and image-guided radiation therapy (IGRT) are introduced into the clinic. As new technologies are introduced, the number and sophistication of possible activities, tests and measurements required to maintain quality also increase.

Therefore, there is a keen need to develop a systematic RTQA program that balances patient safety and quality with available resources and also prescriptiveness with flexibility (13).

PROBLEMS WITH CURRENT RTQA PROGRAMS

The goal of an RTQA program is to deliver the best and safest RT to each patient to achieve cure or palliation. The quality of RT has been defined as the totality of features or characteristics of the RT service that bear on its ability to satisfy the stated or implied goal of effective patient care. The integrated nature of QA in RT makes it impossible to consider QA as limited to simply checking machine output or calibrating brachytherapy sources. QA activities cover a very broad range of areas in which the actions of radiation oncologists, radiation technologists, dosimetrists, accelerator engineers and medical physicists are important. With the increasing complexity of the equipment and processes required to deliver modern RT, the activities required to maintain and enhance quality are consuming ever more resources, and we need to re-examine the amount and distribution of resources committed to QA. In particular, we need to link QA activities to the expected benefit to the patient. In addition to re-examining current practice, the rapid introduction of new advanced technologies poses other challenges. The current process of developing consensus recommendations for prescriptive QA activities remains valid for many of the devices and software systems used in modern RT; however, for some technologies, QA guidance is incomplete or out of date. The formulation of QA guidance lags far behind the penetration of IMRT and IGRT into the community, leaving physicists and radiation oncologists without a clear strategy to maintain the quality and safety of treatment. In addition to leaving practitioners and patients at greater risk of catastrophic delivery errors, data from phantom testing have suggested that the quality of IMRT delivery has been much poorer than that expected (14). In such situations, physicists will be best served by guidance on how to approach the development of a QM system. Even before the availability of advanced technologies such as IMRT and IGRT, it was clear that the treatment preparation and the delivery equipment had such a wide range of possible configurations that both commissioning and routine QA activities could do no more than sample the performance of the equipment under selected conditions. There is a need to re-examine objectively those selected conditions and confirm that they are the most critical for modern RT (15,16).

NEW PARADIGM FOR RTQA

To solve these problems, it is important to evaluate more formal error mitigation and process analysis methods of industrial engineering, such as aircraft accident analysis (17), to focus available QA resources more optimally on process components that have a significant likelihood of compromising patient safety or treatment outcomes.

The new possible approach is based on designing a framework for QM activities with the maximal impact being achieved when resource allocation reflects both the probability of an event and the severity should it occur; this requires quantitative knowledge of both probability and severity. To understand the new approach, new concepts, failure mode and effect analysis (FMEA) need to be

understood (18,19). This is a systematic method for documenting potential failure modes, determining effects, identifying causes of failures, developing plans, team concurrence and taking action. For each potential cause of failure, values are assigned in three categories: *O*, the probability that a specific cause will result in a failure mode; *S*, the severity of the effects resulting from a specific failure mode should it go undetected throughout treatment; and *D*, the probability that the failure mode resulting from the specific cause will go undetected. Convention uses numbers between 1 and 10. The product of these three indices forms the risk probability number ($RPN = O \times S \times D$). When designing a QM program based on the RPN values, resources should be allocated to failure modes with higher RPN values. TG 100 of the AAPM is now working to develop a consistent set of values for *O*, *S* and *D*, and a consistent set of terminology for describing the potential causes of failure and potential effects of failure. TG 100 also suggests that this approach could be a useful framework for the objective analysis of myriad emerging technologies. Adoption of a standard approach to QM would have clear advantages in developing new recommendations efficiently.

On the other hand, the WHO World Alliance for Patient Safety has taken an initiative to address high-risk areas in the RT process of care, complementary to the International Atomic Energy Agency (IAEA)-developed safety measures and other previously developed standards, to address non-equipment, non-system faults associated with RT delivery. An expert group facilitated by the WHO World Alliance for Patient Safety is in the process of developing a guide to identify high-risk practices in RT and to suggest specifically targeted interventions to improve patient safety. A literature review showed that, in the last three decades (1976–2007), >1700 patients were affected and ~2% of patients were reported to have died due to radiation overdose toxicity in middle- and high-income countries in the USA, Latin America, Europe and Asia. Most incidents (~98%) were reported to have occurred in the planning stage during the introduction of new systems and/or equipment. Of all incidents without any known adverse events to patients, 7% were related to the planning stage; 39% were related to information transfer and 19% to the treatment delivery stage. The remaining 35% of incidents occurred in the categories of prescription, simulation, patient positioning or in a combination of multiple stages (personal communication). The report will be published in the near future and will be useful to develop process-oriented RTQA programs.

EXTERNAL PEER REVIEW AUDIT

External audit programs for RTQA can serve to improve patient safety and quality of care. The international basic safety standards (20) require radiation centers to establish comprehensive QA programs for medical exposure, including external auditing for RT. Both regulatory authorities and professional societies have responded, producing similar end products. The Council Directive of the European Community 97/43/European Atomic Energy Community strengthened the need for clinical auditing in Europe. The regulatory authority of Finland (21,22) is pursuing a program to implement the European Union directive in all areas of radiation medicine. Norway's Radiation Protection Authority (23) has reported that 'Clinical audit/review involves mutual learning wherein colleagues evaluate completed work from the perspective of good clinical practice. This is essentially different from an authority's regulatory inspection where practice/activities are evaluated against laws and regulations.' The ESTRO has initiated a process to define comprehensive auditing (24). In all cases, the auditing team is composed of professionals; physician, medical physicist and radiation technologist. The IAEA also introduced its QA Team for Radiation Oncology (QUATRO) (25). The objective of QUATRO auditing is to review and evaluate the quality of the practice of RT at a cancer center to define how best to improve the practice. A guideline document (26) has defined how to conduct the audit. The IAEA has organized several workshops to train QUATRO auditors, and 17 missions were completed as of November 2006 in Europe and Asia. Individual RT centers received recommendations on quality improvement. In eastern European countries, most audited centers operate at a level requiring only minor improvements, except for the general shortage of well-qualified radiation technologists. Two centers were identified as operating at an internationally accepted level (27). Some countries, such as the Czech Republic (28), have adapted the QUATRO approach for national clinical auditing. In Asia, existing structural inadequacies were addressed.

In addition to an on-site audit, an off-site audit, such as a postal dosimetry audit program, is necessary to assure the dose from RT equipment. For more than three decades, the IAEA has operated a postal thermoluminescent dosimetry (TLD) dose-auditing program (29) for more than 1600 RT institutions in 120 countries. A global and steady improvement in the performance of dosimetry audits has been occurring so that ~95% of the participating institutions are within the 5% acceptance limit for beam calibration. Several countries have adopted the IAEA's method to establish their own national auditing networks (30–32). In Japan, a similar postal dosimetry audit program using a glass dosimeter was started on November 2007 (33,34). Further development is being considered to check not only the reference condition, i.e. beam calibration, but also non-reference conditions, such as irregularly shaped and wedged beams.

CLINICAL TRIAL QA

In the USA, RTQA programs have been developed mainly through clinical trial QA. The Radiological Physics Center (RPC) has been funded by the National Cancer Institute (NCI) continually since 1968 to provide quality auditing of

dosimetry practices at institutions participating in NCI cooperative clinical trials. The primary responsibility of the RPC is to assure the NCI and the cooperative clinical trial groups that all participating institutions have the equipment, personnel and procedures necessary to administer radiation doses that are clinically comparable and consistent. The monitoring tools used include on-site dosimetry reviews; remote auditing tools, including TLD and anthropomorphic phantoms; and reviews of both benchmark and actual protocol patient treatments. As of 2007, the RPC monitors nearly 1500 RT institutions. Discrepancies detected by the RPC are investigated to help the institution resolve them. The RPC overall RTQA program has an impact not only on the treatment received by patients enrolled in clinical trials, but also on the quality of treatment administered to all patients treated at the institution.

The NCI-sponsored Advanced Technology QA Consortium (ATC), which consists of the Image-Guided Therapy QA Center (ITC), Radiation Therapy Oncology Group (RTOG), RPC, QA Review Center (QARC) and Resource Center for Emerging Technologies, has pioneered the development of an infrastructure and QA method for advanced technology clinical trials that requires volumetric digital data submission of a protocol patient's treatment plan and verification data. In particular, the ITC has nearly 15 years' experience in facilitating the QA review for RTOG advanced technology clinical trials. This QA process includes: (i) a data integrity review for completeness of protocol-required elements, the format of data, and possible data corruption, and recalculation of dose–volume histograms, (ii) a review of compliance with target volume and organ-at-risk contours by study chairs and (iii) a review of dose prescription and dose heterogeneity compliance by the RTOG Headquarters Dosimetry Group.

They also require institutions to obtain credentials before participating in clinical trials. The concepts pioneered by the ITC and RTOG include: (i) a facility questionnaire that documents the institution's technical capabilities and identifies the critical treatment team individuals and (ii) a series of tests that are protocol modality-specific, including an electronic data submission test and a dry-run test, to demonstrate understanding of the protocol planning and data submission requirements. New modalities such as IMRT and Stereotactic Body Radiation Therapy (SBRT) require additional credential tests. The RPC developed a postal anthropomorphic phantom (Fig. 2) that contains dosimeters to test the delivery capabilities of the institutions' IMRT systems (35) and a localization credential test has been implemented for SBRT protocols to test the reproducibility of the patient setup (36). The primary goal of credentials is to reduce the deviation rate for data submitted to clinical trials. Cooperative groups have experienced deviation rates that sometimes amount to as much as 17% of the cases submitted, according to a study conducted by the RPC (37). An elevated number of deviations reduce the quality of the study, and increased rates of major deviations may limit

Figure 2. The Radiological Physics Center postal anthropomorphic phantom.

accrual to the trial. Credentialing evaluations result in feedback to the institution, to explain the results of the procedure and to give suggestions to improve those results in the future. Three protocols for which credentialing was required from all participants had rates of deviation between 0 and 4%, whereas two protocols that had limited credential requirements had rates of deviation of the order of 7–17% (37,38).

These activities have also been adopted in Europe and Japan. As early as in 1982, the European Organization for Research and Treatment of Cancer RT Group (EORTC) established RTQA programs. In the course of 25 years, QA procedures have become a vast and important part of the activities of the group. The radiation dosimetry QA program demonstrated the disappearance of large deviations of photon and electron beam calibrations after two successive audits (39). This methodology has now become a standard procedure in RT routine practice in Europe. In Japan, following the results of a phase III trial that revealed poor protocol compliance (40%), the Japan Clinical Oncology Group (JCOG) started clinical trial RTQA programs in 2002 (40,41). The QA scores of the first trial (JCOG 0202) that required on-going RTQA have been reported recently and showed good protocol compliance (42). The JCOG is also collaborating with the ATC and EORTC to establish a global standard in advanced technology clinical trial QA. A phase II SBRT trial for stage I non-small cell lung cancer (JCOG 0403) is supported by the ATC (43) and individual case reviews are being performed using a web-based remote review tool (Fig. 3).

CONCLUSIONS

Recent advances in RT focus on the need for a systematic RTQA program that balances patient safety and quality with

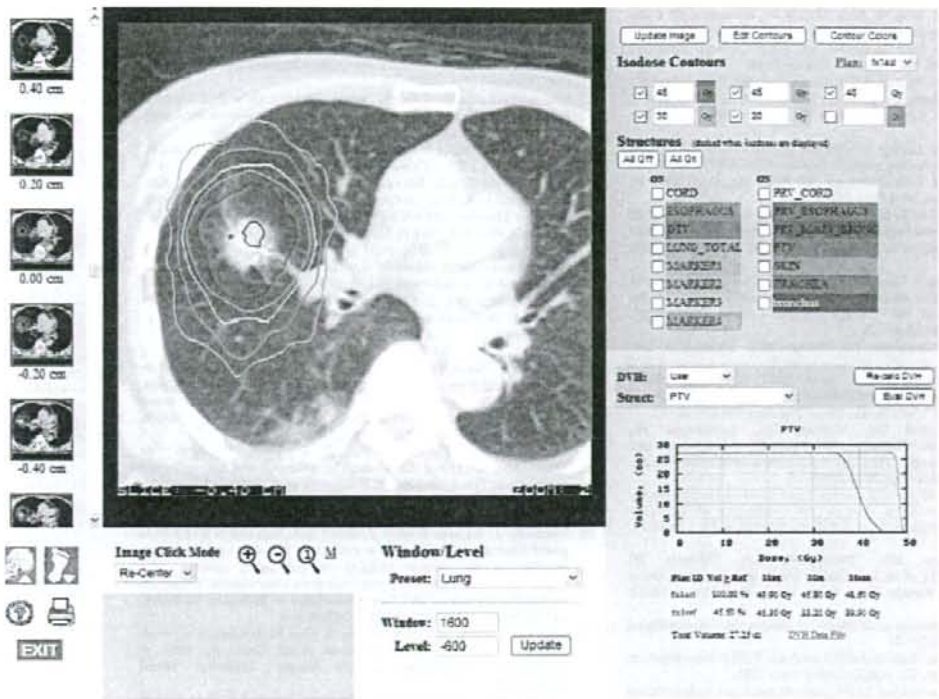

Figure 3. Advanced Technology Quality Assurance Consortium remote review tool.

available resources. It is necessary to develop more formal error mitigation and process analysis methods such as FMEA to focus available QA resources more optimally on process components to avoid catastrophic delivery errors. External audit programs for RTQA are also effective. Both postal dosimetry audit and clinical trial RTQA, especially for advanced technologies, in collaboration with global networks, will serve to enhance patient safety and quality of care.

Conflict of interest statement

None declared.

References

1. Matsuda T, Marugame T, Kamo K, Katanoda K, Ajiki W, Sobue T, et al. Cancer incidence and incidence rates in Japan in 2002: based on data from 11 population-based cancer registries. Jpn J Clin Oncol 2008; 38:641–8.
2. JASTRO database committee. Present status of radiotherapy in Japan: the regular structure survey in 2003. J Jpn Soc Ther Radiol Oncol 2005;15:115–21 (in Japanese).
3. Delaney G, Jacob S, Featherstone C, Barton M. The role of radiotherapy in cancer treatment: estimating optimal utilization from a review of evidence-based clinical guidelines. Cancer 2005;104: 1129–37.
4. Tripartite committee - The Faculty of Radiation Oncology, The Australian Institute of Radiography, The Australasian College of Physical Scientists and Engineers in Medicine. Developing standards for radiation treatment services in Australia. Sydney: RANZCR 2005. Available at: http://www.ranzcr.edu.au/documents/download.cfm/Discussion%20Paper%20-%20Final.pdf?txtLibraryID=ranzcr&txtFileName=ACF4E02.pdf (Accessed 18 August 2008).
5. Kutcher GJ, Coia L, Gillin M, Hanson WF, Leibel S, Morton RJ, et al. Comprehensive QA for radiation oncology: Report of AAPM Radiation Therapy Committee Task Group 40. Med Phys 1994;21: 581–618.
6. Rivard MJ, Coursey BM, DeWerd LA, Hanson WF, Huq MS, Ibbott GS, et al. Update of AAPM Task Group No. 43 report: a revised AAPM protocol for brachytherapy dose calculations. Med Phys 2004;31:633–74.
7. Fraass B, Doppke K, Hunt M, Kutcher G, Starkschall G, Stern R, et al. American Association of Physicists in Medicine Radiation Therapy Committee Task Group 53: quality assurance for clinical radiotherapy treatment planning. Med Phys 1998;25:1773–829.

8. Nath R, Anderson LL, Meli JA, Olch AJ, Stitt JA, Williamson JF. Code of practice for brachytherapy physics: Report of the AAPM Radiation Therapy Committee Task Group No. 56. American Association of Physicists in Medicine. Med Phys 1997;24:1557–98.
9. Kubo HD, Glasgow GP, Pethel TD, Thomadsen BR, Williamson JF. High dose-rate brachytherapy treatment delivery: Report on the AAPM Radiation Therapy Committee Task Group no. 59. Med Phys 1998;25:375–403.
10. Nath R, Amols H, Coffey C, Duggan D, Jani S, Li Z, et al. Intravascular brachytherapy physics: Report of the AAPM Radiation Therapy Committee Task Group no. 60. American Association of Physicists in Medicine. Med Phys 1999;26:119–52.
11. Yu Y, Anderson LL, Li Z, Mellenberg DE, Nath R, Schell MC, et al. Permanent prostate seed implant brachytherapy: Report of the American Association of Physicists in Medicine Task Group No. 64. Med Phys 1999;26:2054–76.
12. Thwaites D, Scalliet P, Leer JW, Overgaard J. Quality assurance in radiotherapy. ESTRO advisory report to the Commission of the European Union for the 'Europe Against Cancer Programme'. Radiother Oncol 1995;35:61–73.
13. Williamson JF, Dunscombe PB, Sharpe MB, Thomadsen BR, Purdy JA, Deye JA. Quality assurance needs for modern image-based radiotherapy: recommendations from 2007 interorganizational symposium on "quality assurance of radiation therapy: challenges of advanced technology". Int J Radiat Oncol Biol Phys 2008;71:S2–12.
14. Ibbott GS, Followill DS, Molineu HA, Lowenstein JR, Alvarez PE, Roll JE. Challenges in credentialing institutions and participants in advanced technology multi-institutional clinical trials. Int J Radiat Oncol Biol Phys 2008;71:S71–5.
15. Palta JR, Liu C, Li JG. Current external beam radiation therapy quality assurance guidance: Does it meet the challenges of emerging image-guided technologies? Int J Radiat Oncol Biol Phys 2008;71: S13–7.
16. Huq MS, Fraass BA, Dunscombe PB, Gibbons JP, Ibbott GS, Medin PM, et al. A method for evaluation quality assurance needs in radiation therapy. Int J Radiat Oncol Biol Phys 2008;71: S170–3.
17. Logan T. Error prevention as developed in airlines. Int J Radiat Oncol Biol Phys 2008;71:S178–81.
18. Stamatis DH. Failure mode and effect analysis: FMEA from theory to execution. Milwaukee, WI: ASQC Quality Press 1995.
19. Rath F. Tools for developing a QM program: proactive tools (process mapping, value stream mapping, fault tree analysis and Failure Mode and Effects Analysis (FMEA). Int J Radiat Oncol Biol Phys 2008; 71:S187–90.
20. International Atomic Energy Agency. International Basic Safety Standards for Protection Against Ionizing Radiation and for the Safety of Radiation Sources. IAEA Safety Series No. 115. Vienna: IAEA 1996.
21. Soimakallioa S, Järvinen H, Ahonen A, Wigren T, Lyyra-Laitinen T. Impact of clinical audit on the quality of radiological practices—experiences from a national audit programme supported by a national steering committee. In: Shortt KR editor. Book of Extended Synopses. International Conference on Quality Assurance and New Techniques in Radiation Medicine. IAEA-CN-146/038. Vienna: IAEA 2006;104–5.
22. Parkkinen R, Järvinen H. Implementation of QA in medical radiological practices: a national cooperation model. In: Shortt KR editor. Book of Extended Synopses. International Conference on Quality Assurance and New Techniques in Radiation Medicine. IAEA-CN-146/139P. Vienna: IAEA 2006,114–5.
23. Norwegian Radiation Protection Authority Bulletin. Quality assurance in radiotherapy. Østera's: Norwegian Radiation Protection Authority 2005.
24. Malicki J, Järvinen H, Scalliet P, Stankusová H, Leer JW. Clinical audit guidelines in radiotherapy -Preliminary results of the ESTRO working group. In: Shortt KR editor. Book of Extended Synopses. International Conference on Quality Assurance and New Techniques in Radiation Medicine. IAEA-CN-146/039. Vienna: IAEA 2006,106–7.
25. Izewska J, Scalliet P, Levin V, Järvinen H, Lartigau E. QA team for radiation oncology (QUATRO). In: Shortt KR editor. Book of Extended Synopses. International Conference on Quality Assurance and New Techniques in Radiation Medicine. IAEA-CN-146/036. Vienna: IAEA 2006,100–1.
26. International Atomic Energy Agency. Comprehensive Audits of Radiotherapy Practice: A Tool for Quality Improvement. STI/PUB/ 1297. Vienna: IAEA 2007.
27. International Atomic Energy Agency. Setting up a Radiotherapy Programme: Clinical, Medical Physics, Radiation Protection and Safety Aspects. STI/PUB/1296. Vienna: IAEA 2008.
28. Horáková I, Pavlíková I, Valenta J, Petera J, Šlampa P, Stankusová H. Components of QA of radiotherapy process—setup in the Czech Republic. In: Shortt KR editor. Book of Extended Synopses. International Conference on Quality Assurance and New Techniques in Radiation Medicine. IAEA-CN-146/138P. Vienna: IAEA 2006,112–3.
29. Izewska J, Georg D, Bera P, Thwaites DI, Arib M. Development of a methodology for TLD postal dosimetry audit of high-energy radiotherapy photon beams in non-reference conditions: an IAEA coordinated research project. In: Shortt KR editor. Book of Extended Synopses. International Conference on Quality Assurance and New Techniques in Radiation Medicine. IAEA-CN-146/088. Vienna: IAEA 2006,408–9.
30. Sergieva KM, Buchakliev Z, Ivanov G, Dimitrova V, Staykova V, Gesheva N. The results from external TLD audit in reference and non-reference conditions in Bulgarian radiotherapy centres. In: Shortt KR editor. Book of Extended Synopses. International Conference on Quality Assurance and New Techniques in Radiation Medicine. IAEACN-146/227P. Vienna: IAEA 2006,416–7.
31. Viamonte A, Viegas CCB, Rosa LAR, Campos de Araujo AM, Souza RS. Postal audit in reference and non-reference conditions in Brazil. In: Shortt KR editor. Book of Extended Synopses. International Conference on Quality Assurance and New Techniques in Radiation Medicine. IAEA-CN-146/229P. Vienna: IAEA 2006,420–1.
32. Vatnitsky S, Izewska J, Bera P, Shortt KR. The IAEA/WHO TLD postal dose audits as a tool for evaluating the status of dosimetry practices in radiotherapy hospitals in developing countries. In: Shortt KR editor. Book of Extended Synopses. International Conference on Quality Assurance and New Techniques in Radiation Medicine. IAEA-CN-146/234P. Vienna: IAEA 2006,430–1.
33. Mizuno H, Kanai T, Kusano Y, Ko S, Ono M, Fukumura A, et al. Feasibility study of glass dosimeter postal dosimetry audit of high-energy radiotherapy photon beams. Radiother Oncol 2008;86:258–63.
34. Cancer Control and Information Services, National Cancer Center. Remote and on-site radiotherapy audit program. Available at: http:// www.ncc.go.jp/jp/cis/divisions/01clinical/clinicaltest05_en.html (Accessed 18 August 2008).
35. Molineu A, Followill DS, Balter PA, Hanson WF, Gillin MT, Huq MS, et al. Design and implementation of an anthropomorphic quality assurance phantom for intensity-modulated radiation therapy for the Radiation Therapy Oncology Group. Int J Radiat Oncol Biol Phys 2005;63:577–83.
36. Radiation Therapy Oncology Group. RTOG 0236: a phase II trial of stereotactic body radiation therapy (SBRT) in the treatment of patients with medically inoperable stage I/II non-small cell lung cancer. 2002. Available at: http://www.rtog.org/members/protocols/0236/0236.pdf (Accessed 18 August 2008).
37. Leif J, Roll J, Followill D, Ibbott G. The value of credentialing. Int J Radiat Oncol Biol Phys 2006;66:S716.
38. Ibbott GS, Hanson WF, O'Meara E, Kuske RR, Arthur D, Rabinovitch R, et al. Dose specification and quality assurance of Radiation Therapy Oncology Group protocol 95-17: A cooperative group study of 192Ir breast implants as sole therapy. Int J Radiat Oncol Biol Phys 2007;69:1572–8.
39. Bernier J, Horiot JC, Poortmans P. Quality assurance in radiotherapy: from radiation physics to patient and trial-oriented control procedures. Eur J Cancer 2002;38:S155–8.
40. Atagi S, Kawahara M, Tamura T, Noda K, Watanabe K, Yokoyama A, et al. Standard thoracic radiotherapy with or without concurrent daily low-dose carboplatin in elderly patients with locally advanced non-small cell lung cancer: a phase III trial of the Japan Clinical Oncology Group (JCOG9812). Jpn J Clin Oncol 2005;35:195–201.
41. Ishikura S, Teshima T, Ikeda H, Hayakawa K, Hiraoka M, Atagi S, et al. Initial experience of quality assurance in radiotherapy within the